Nematic fluctuations in iron arsenides NaFeAs and LiFeAs probed by ^{75}As NMR

Masayuki Toyoda, Yoshiaki Kobayashi, and Masayuki Itoh
Department of Physics, Graduate School of Science, Nagoya University, Furo-cho, Chikusa-ku, Nagoya 464-8602, Japan

(Received 14 November 2017; revised manuscript received 23 February 2018; published 26 March 2018)

^{75}As NMR measurements have been made on single crystals to study the nematic state in the iron arsenides NaFeAs, which undergoes a structural transition from a high-temperature (high-T) tetragonal phase to a low-T orthorhombic phase at $T_s = 57$ K and an antiferromagnetic transition at $T_N = 42$ K, and LiFeAs having a superconducting transition at $T_c = 18$ K. We observe the in-plane anisotropy of the electric field gradient η even in the tetragonal phase of NaFeAs and LiFeAs, showing the local breaking of tetragonal C_4 symmetry. Then, η is found to obey the Curie-Weiss (CW) law as well as in $Ba(Fe_{1-x}Co_x)_2As_2$. The good agreement between η and the nematic susceptibility obtained by electronic Raman spectroscopy indicates that η is governed by the nematic susceptibility. From comparing η in NaFeAs and LiFeAs with η in $Ba(Fe_{1-x}Co_x)_2As_2$, we discuss the carrier-doping dependence of the nematic susceptibility. The spin contribution to nematic susceptibility is also discussed from comparing the CW terms in η with the nuclear spin-lattice relaxation rate divided by temperature $1/T_1T$. Finally, we discuss the nematic transition in the paramagnetic orthorhombic phase of NaFeAs from the in-plane anisotropy of $1/T_1T$.

DOI: 10.1103/PhysRevB.97.094515

I. INTRODUCTION

Understanding an exotic electronic state is one of the central issues in condensed matter physics. Recently, one of these exotic electronic states, a nematic electronic state, where rotational symmetry is broken but translational symmetry is preserved, has attracted much attention in Fe-based superconductors [1–4]. The nematic state appears with C_4 symmetry breaking even in the tetragonal phase of Fe-based superconductors. The origin of the nematic state is also considered to be closely related to the superconducting (SC) mechanism, the magnetic or orbital fluctuations.

The presence of a nematic state was first detected in resistivity measurements on $Ba(Fe_{1-x}Co_x)_2As_2$ under a uniaxial stress where C_4 symmetry within the FeAs plane is broken even in the tetragonal phase [5]. Furthermore, angle-resolved photoemission spectroscopy (ARPES) showed the degeneracy of the Fe $3d_{xz}$ and $3d_{yz}$ orbitals is lifted even in its tetragonal phase [6]. In addition to those studies, the nematic state has been investigated by several techniques such as shear modulus C_{66} [7–10], strain-dependent resistivity [11], electronic Raman response function [12], and stress-dependent optical reflectivity [13] measurements. Therefore, nematic susceptibility governed by nematic fluctuations is a crucial measure to study nematic phenomena [14]. Based on the results of the nematic susceptibility obtained by experimental methods such as C_{66} and electron Raman measurements, the nematic transition is discussed as an important issue, with regards as to whether or not the nematic transition drives the structural transition. From a theoretical point of view, spin-nematic [7,15–19] and orbital-nematic [20–26] scenarios are proposed as an origin of the nematic order and the nematic transition. The former is based on the primary instability in the spin fluctuation with the wave vectors $\mathbf{Q}_X = (\pi,0)$ and $\mathbf{Q}_Y = (0,\pi)$, among which the stripe-type magnetic order appears with $\mathbf{Q}_X$ in the antiferromagnetic (AFM) phase, whereas the nematic order parameter in the latter scenario is the difference in orbital occupancy. Nematic susceptibility is calculated on the basis of both scenarios to reproduce the Raman and C_{66} results. In spite of such extensive studies, nematic phenomena remain insufficiently understood and various experimental methods are required to clarify their characteristics.

Nuclear magnetic resonance (NMR) is a powerful tool to study the local magnetic and electric properties of Fe-based superconductors [27,28]. There are also reports on nematic phenomena observed via magnetic hyperfine and electrical quadrupole interactions. From measurements of the ^{77}Se Knight shift, nematic phenomena were discussed to appear in FeSe [29–31]. Based on NMR spectra at high pressure, static and local nematic ordering was also reported to exist well above the bulk nematic ordering temperature in FeSe [32,33]. On the other hand, from the observation of anisotropy in the electric field gradient (EFG), in-plane anisotropy was reported to appear even in the tetragonal phase of $Ba(Fe_{1-x}Co_x)_2As_2$ [34–36] and $NaFe_{1-x}Co_xAs$ [37]. Also, the in-plane anisotropy observed in $BaFe_2(As_{1-x}P_x)_2$ was concluded to provide evidence of a population imbalance between As $4p_x$ and $4p_y$ orbitals, which is a natural consequence of the orbital ordering of Fe $3d_{xz}$ and d_{yz} electrons [38]. Recently, the local nematic susceptibility was measured from electric quadrupole splitting under a strain field in $BaFe_2As_2$ [39]. Also, based on nuclear spin-lattice relaxation, glassy nematic fluctuations in $Ba(Fe_{1-x}Co_x)_2As_2$ [40,41] and $BaFe_2(As_{1-x}P_x)_2$ [42] were discussed. Thus, measurements of the EFG parameters which can directly monitor the charge degrees of freedom allow us to access the nematic susceptibility. To systematically investigate nematic susceptibility via the NMR technique, careful EFG measurements using single crystals are desired on various

Fe-based superconductors, such as the 111-type compounds NaFeAs and LiFeAs, in addition to the 122-type system $BaFe_2As_2$.

NaFeAs and LiFeAs crystallize in a tetragonal structure (space group $P4/nmm$) at room temperature [43,44]. NaFeAs undergoes a structural transition from a high-temperature (high-T) tetragonal phase to a low-T orthorhombic phase (space group $Cmma$) at $T_s \sim 54$ K and an AFM transition at $T_N \sim 40$ K [45]. On the other hand, LiFeAs has neither a structural or magnetic transition and undergoes an SC transition at $T_c \sim 18$ K [46]. Thus a comparison between both arsenides is useful to study the effect of the structural transition on the nematic state. Up to now, results of the Knight shift and the nuclear spin-lattice relaxation rate $1/T_1$ were reported for NaFeAs [28,47–49], Co-doped or pressure-applied NaFeAs [37,50,51], LiFeAs [28,52–56], and $LiFe_{1-x}Co_xAs$ [57] from several NMR and nuclear quadrupole resonance (NQR) studies. The structural transition associated with the nematic order in NaFeAs was also monitored by EFG measurements [28,47–49].

In this paper, we have performed ^{75}As NMR measurements on single crystals to study the nematic state via the in-plane anisotropy of the EFG tensor η in the iron arsenides NaFeAs and LiFeAs. We observe nonzero η even in the tetragonal phase of both NaFeAs and LiFeAs. This clearly shows that in-plane anisotropy locally breaks tetragonal C_4 symmetry. Furthermore, we observe that η obeys the Curie-Weiss (CW) law in the tetragonal phase of NaFeAs and LiFeAs as well as in $Ba(Fe_{1-x}Co_x)_2As_2$. A comparison between η and the electronic Raman data indicates that η monitors the nematic susceptibility. The spin contribution to nematic susceptibility is also discussed from comparing the CW terms in η and the nuclear spin-lattice relaxation rate divided by temperature $1/T_1T$. We also discuss the nematic order via the anisotropy of $1/T_1T$ in the paramagnetic orthorhombic phase of NaFeAs.

II. EXPERIMENTAL PROCEDURE

NaFeAs and LiFeAs single crystals used in the present NMR experiments were prepared by the self-flux method [58]. Fe powders, As powders, and A (=Na and Li) lumps were mixed in a molar ratio of $A : Fe : As = 3 : 2 : 3$. The mixture was put in a boron nitride crucible and sealed in an evacuated quartz tube. It was heated up to 900 °C for NaFeAs and 1100 °C for LiFeAs at a rate of 30 °C/h, kept for 15 h, and cooled down to 600 °C at a rate of 4.5 °C/h. After cooling it in a furnace, a single crystal of NaFeAs was obtained. For LiFeAs, the quartz tube was turned over to remove the liquid flux at 600 °C, and it was left in the furnace for 6 h. Finally, we obtained single crystals of LiFeAs. For the present NMR experiments, a single crystal of NaFeAs or LiFeAs of a size $2 \times 2 \times 0.1$ mm^3 was put in an NMR coil and sealed in high-purity Ar gas with stycast 1266 to avoid damaging it due to air and moisture. Since the sample is not fixed in the NMR coil by any grease, there is only external stress coming from the NMR coil which attaches the sample.

Magnetic susceptibility was measured using a superconducting interference device magnetometer (SQUID, Quantum Design, MPMS). ^{75}As NMR measurements were made using a conventional pulsed spectrometer. Fourier-transformed spectra were obtained for spin-echo signals in a magnetic field of $H_0 = 7.7028$ or 7.7023 T. An ^{75}As nucleus has a nuclear spin $I = 3/2$ and a nuclear gyromagnetic ratio of $\gamma_n = 2\pi \times 7.2919$ MHz/T. A two-axis goniometer was utilized to precisely rotate the single crystal in the magnetic field. The ^{75}As nuclear spin-lattice relaxation rate $1/T_1$ was measured by the inversion-recovery method.

III. EXPERIMENTAL RESULTS

A. NaFeAs

Figure 1 shows the T dependence of the ^{75}As NMR spectrum with $H_0 = 7.7028$ T parallel to the Fe-Fe direction (the a or b direction in the orthorhombic axis) in NaFeAs. In the tetragonal phase above $T_s = 57.0$ K, it has one center and two satellite lines split by the electric quadrupole effect. Each of the center and satellite lines is clearly split into two lines due to the orthorhombic twin structure in the paramagnetic orthorhombic phase in the T range from T_s to $T_N = 42.0$ K. In the AFM phase, the two center lines become broad and overlapped, whereas each of the two lines in the upper and lower satellites becomes slightly broadened. These spectra are well explained by stripe-type magnetic order [47]. These NMR results are consistent with previous reports [37,47].

We concentrate our attention on the satellite lines which provide information of the EFG tensor. For $I = 3/2$, in the first-order perturbation of the electric quadrupole interaction, electric quadrupole splitting $\delta\nu$ is expressed as

$$\delta\nu = \tfrac{1}{2}\nu_Q(3\cos^2\theta - 1 + \eta\sin^2\theta\cos 2\phi), \quad (1)$$

where θ is the polar angle from the principal z axis, ϕ is the azimuth angle from the principal x axis in the xyz principal coordinate system of the EFG tensor, and ν_Q ($=|\nu_z| = |\nu_x + \nu_y|$) is the nuclear electric quadrupole frequency with the maximum principal value of the EFG tensor $V_{\alpha\alpha}$ ($\alpha = x$, y, and z) [59]. Here, we define ν_α as $\nu_\alpha = 3eQV_{\alpha\alpha}/[2I(2I-1)h]$ with the elementary charge e, the nuclear quadrupole moment Q, and the Planck's constant h. Also, the asymmetry parameter of EFG is defined as $\eta = |\nu_x - \nu_y|/|\nu_z|$.

In the orthorhombic phase below T_s, the splitting of the satellite line with H_0 rotated in the c plane is clearly observed, as seen in Fig. 1(b), where the angle ϕ dependence of the satellite line at 50 K is displayed. Here, ϕ is measured from the Fe-Fe direction parallel to the a or b axis in the c plane ($\theta = \pi/2$). As presented in the inset of Fig. 1(b), the two lines coming from the twin structure with the a or b axis normal to each other in the orthorhombic phase show the ϕ dependence governed by $(|\nu_x|,|\nu_y|) = (4.438,5.412)$ MHz $= (|\nu_a|,|\nu_b|)$ or $(|\nu_b|,|\nu_a|)$, $\nu_z = \nu_c$, and $\eta = 0.0990$, which agree with the reported values [37,48]. The a and b axes are not identified in the present experiment. On the other hand, in the tetragonal phase, the space group $P4/nmm$ requires $\eta = 0$ and $\nu_Q = |\nu_c|$. However, each satellite line is almost composed of two Gaussians, A and B, with the same intensity and the same full width at half maximum (FWHM) of 0.086 MHz, as presented in Fig. 1(c), which shows the ϕ dependence of the lower and upper satellite lines in the c plane at 180 K. The presence of A and B spectra is ascribed to two regions with local symmetry axes perpendicular to each other, namely, the local orthorhombic a or b axes parallel to the Fe-Fe direction.

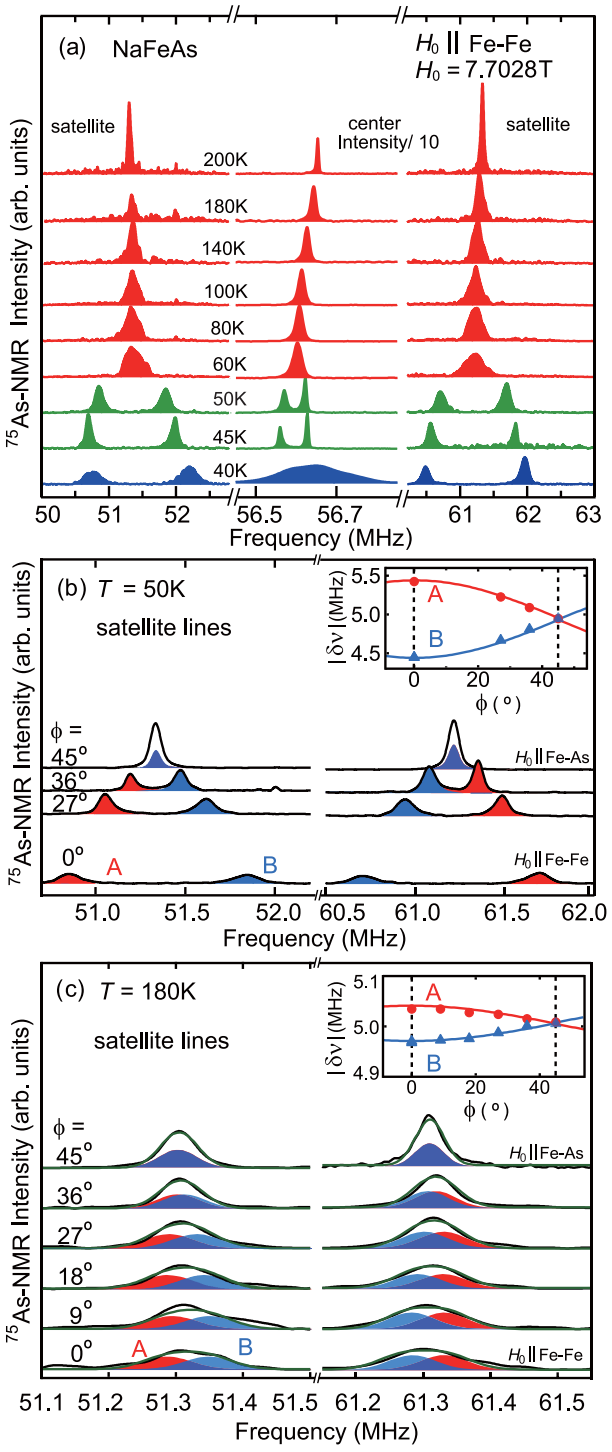

FIG. 1. (a) Temperature dependence of the ^{75}As NMR spectrum with $H_0 = 7.7028$ T parallel to the Fe-Fe direction in single-crystalline NaFeAs. Angle ϕ dependence of the ^{75}As NMR spectrum (b) at 50 K in the orthorhombic phase and (c) at 180 K in the tetragonal phase with H_0 rotated in the c plane. The NMR spectrum is composed of A (red) and B (blue) spectra in (b), whereas it can be reproduced by the summation (green) of two Gaussians A (red) and B (blue) in (c). The insets show the ϕ dependence of the electric quadrupole splitting $|\delta\nu|$ with H_0 rotated in the c plane. The angle ϕ is measured from the Fe-Fe direction corresponding to the orthorhombic a or b axis. The Fe-As direction is defined as the direction of the Fe-As bond projected on the c plane.

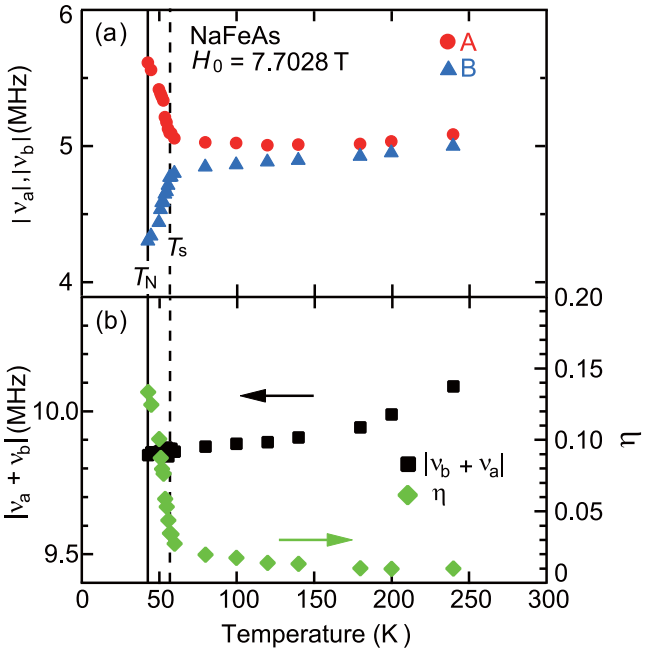

FIG. 2. Temperature dependences of (a) the ^{75}As nuclear quadrupole frequency $|\nu_\alpha|$ ($\alpha = a$ and b), and (b) $|\nu_a + \nu_b|$ ($=|\nu_c|$) and the asymmetry parameter of the electric field gradient tensor η in single-crystalline NaFeAs. T_s (=57.0 K) and T_N (=42.0 K) are the structural-transition temperature and the Néel temperature, respectively.

This angular dependence provides $|\nu_x| = 4.968$ MHz, $|\nu_y| = 5.033$ MHz, and $\eta = 0.0065$, where the x (y) axis is the a (b) or b (a) axis. Thus these results clearly show that tetragonal C_4 symmetry is locally broken even in the tetragonal phase of NaFeAs.

Figure 2(a) shows the T dependences of $|\nu_a|$ and $|\nu_b|$ in single-crystalline NaFeAs. The difference between $|\nu_a|$ and $|\nu_b|$ increases with decreasing T from 300 K to T_s in the tetragonal phase and increases more rapidly below T_s. The characteristics of the anisotropic behavior of EFG are more clearly seen in Fig. 2(b), which shows the T dependences of $|\nu_a + \nu_b|$ ($=\nu_Q$) and η ($=|\nu_a - \nu_b|/|\nu_a + \nu_b|$). Note that η remains nonzero even at 240 K above T_s. Below T_s, ν_Q slightly changes, whereas η rapidly increases with decreasing T, obeying the T dependence of the order parameter in the structural transition as seen in Fig. 2(b).

In the orthorhombic phase, the nematic transition was observed to provide the in-plane anisotropy in $1/T_1T$. In Fig. 3(a), we present the T dependences of magnetic susceptibility χ and its T derivative $d\chi(T)/dT$ to confirm T_s and T_N in the present NaFeAs sample. Here, $T_s = 57.0$ K is defined as the temperature below which $d\chi(T)/dT$ approximately starts to change with η due to the structural transition, whereas $T_N = 42.0$ K is defined from the maximum of $1/T_1T$ due to the critical slowing down toward T_N. The T_s value is consistent with the reported values determined by ^{23}Na NMR measurements [28,47,49]. We obtained the T_1 values by fitting the experimental data of the nuclear magnetization decay after the inversion pulse $P(t) = [M(\infty) - M(t)]/[2M(\infty)]$, where $M(t)$ is the ^{75}As nuclear magnetization at a time t after an

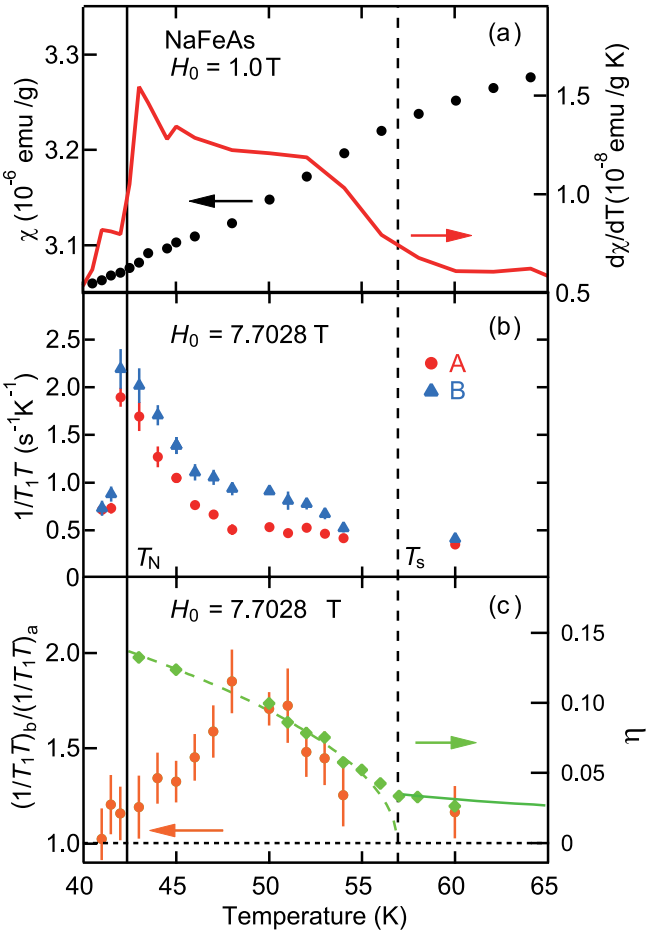

FIG. 3. Temperature dependences of (a) magnetic susceptibility χ and its T derivative $d\chi(T)/dT$ measured for $H_0(=1.0\ \mathrm{T})\|c$, (b) the ^{75}As nuclear spin-lattice relaxation rate divided by T, $1/(T_1T)$, for the A and B satellites with $H_0 = 7.7028$ T parallel to the Fe-Fe direction, and (c) $(1/T_1T)_b/(1/T_1T)_a$ in single-crystalline NaFeAs. In (c), the experimental data of η are well traced by the dashed green curve $\eta \propto \sqrt{1 - T/T_s}$ below $T_s = 57.0$ K, whereas the T dependence of η with the result (solid green curve) of fitting the data above 60 K to the Curie-Weiss law (see Fig. 6) is presented for comparison. T_s and T_N (=42.0 K) are the structural-transition temperature and the Néel temperature, respectively.

inversion pulse, to the theoretical equation,

$$P(t) = 0.1\exp\left(-\frac{t}{T_1}\right) + 0.5\exp\left(-\frac{3t}{T_1}\right) + 0.4\exp\left(-\frac{6t}{T_1}\right), \quad (2)$$

which is applicable to the satellite line well split by the electric quadrupole effect for $I = 3/2$ [60]. Figure 3(b) shows the T dependence of $1/T_1T$ for the A and B lines with $H_0 = 7.7028$ T parallel to the Fe-Fe direction in single-crystalline NaFeAs. Above T_s, $1/T_1T$ shows a slight difference for the A and B lines. With cooling below T_s, after $1/T_1T$ increases and becomes almost T independent down to ~48 K, it shows an increase due to the critical slowing down of spin fluctuations toward T_N. The anisotropy of $1/T_1T$ for the a and b axes in the orthorhombic phase is more clearly seen in Fig. 3(c), where

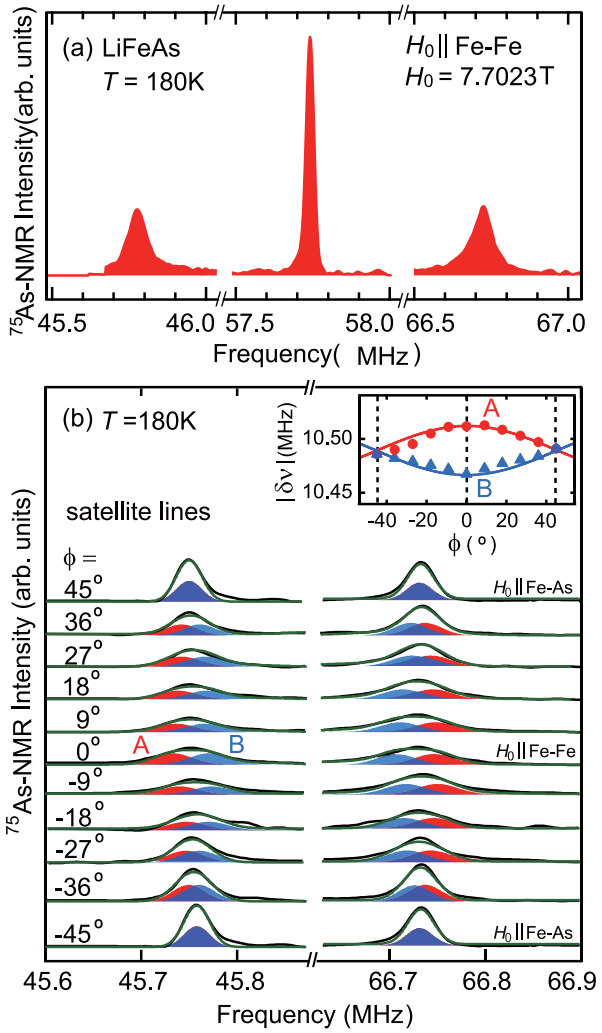

FIG. 4. (a) ^{75}As NMR spectrum at 180 K with $H_0 = 7.7023$ T parallel to the Fe-Fe direction in single-crystalline LiFeAs. (b) Angle ϕ dependence of the lower and upper satellite lines in the NMR spectrum at 180 K with H_0 rotated in the c plane. The NMR spectrum can be reproduced by the summation (green) of two Gaussians A (red) and B (blue) in (b). The inset shows the ϕ dependence of the electric quadrupole splitting $|\delta\nu|$ with H_0 rotated in the c plane. The angle ϕ is measured from the Fe-Fe direction corresponding to the orthorhombic a or b axis. The Fe-As direction is defined as the direction of the Fe-As bond projected on the c plane.

the T dependence of $(1/T_1T)_b/(1/T_1T)_a$ is presented. After the ratio $(1/T_1T)_b/(1/T_1T)_a$ shows a maximum at ~49 K, it reduces toward unity. This means the anisotropy in the FeAs plane vanishes around T_N.

B. LiFeAs

Figure 4(a) shows the ^{75}As NMR spectrum at 180 K with $H_0 = 7.7023$ T parallel to the Fe-Fe direction in single-crystalline LiFeAs. The spectrum has one center and two satellite lines split by the electric quadrupole interaction as well as in the tetragonal phase of NaFeAs. Each satellite line is composed of two Gaussians A and B with the same intensity and the same FWHM of 0.049 MHz, as presented in Fig. 4(b), where the angle ϕ dependence of the satellite

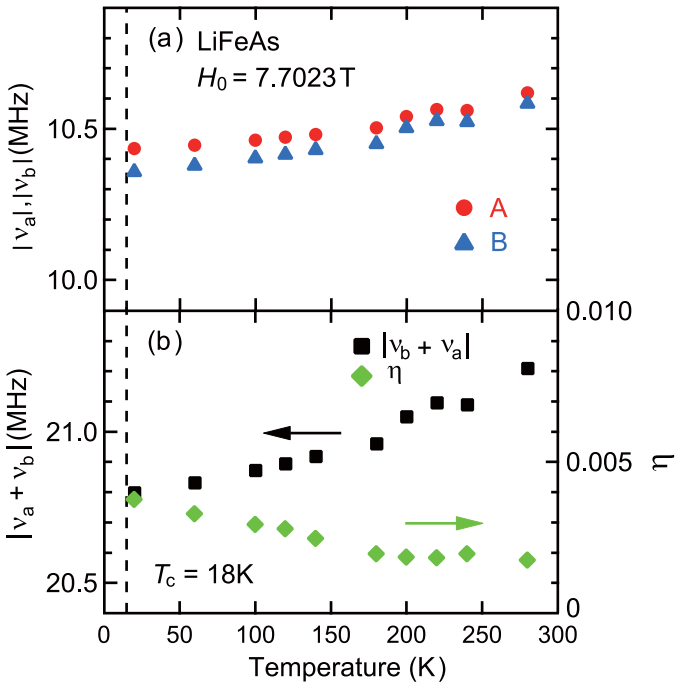

FIG. 5. Temperature dependences of (a) the nuclear quadrupole frequency $|\nu_a|$ and $|\nu_b|$, and (b) $|\nu_a + \nu_b|$ $(=\nu_Q)$ and the nuclear asymmetry parameter of the electric field gradient tensor η in single-crystalline LiFeAs. T_c (=18 K) is the superconducting transition temperature.

lines in the c plane at 180 K is shown and the inset presents the ϕ dependence of the nuclear quadrupole splitting of the two Gaussians $|\delta\nu|$. This angular dependence clearly shows the local breaking of C_4 symmetry in the c plane as well as in the tetragonal phase of NaFeAs. From this angular dependence, we obtain $(|\nu_x|, |\nu_y|) = (10.468, 10.517)$ MHz $= (|\nu_a|, |\nu_b|)$ or $(|\nu_b|, |\nu_a|)$, $\nu_z = \nu_c$, and $\eta = 0.0023$, much smaller than the η value in NaFeAs. The a and b axes are not identified in the present experiment. Figure 5(a) presents the T dependences of $|\nu_a|$ and $|\nu_b|$ in LiFeAs. The difference between $|\nu_a|$ and $|\nu_b|$ increases with decreasing T from 300 K to $T_c = 18$ K. On the other hand, Fig. 5(b) displays the T dependences of $|\nu_a + \nu_b|$ $(=\nu_Q)$ and the asymmetry parameter η in LiFeAs. The ν_Q data agree with the reported result [55]. In particular, note that η is not zero even at 270 K as well as in NaFeAs. Also, η slightly increases with decreasing T in the T range of $T_c < T < 300$ K.

IV. DISCUSSION

A. Asymmetry parameter of electric field gradient η

Based on the present NMR results, we discuss η which can monitor the in-plane anisotropy of the electronic state in the tetragonal phase of NaFeAs and LiFeAs. The observed satellite line of the NMR spectrum reproduced with two Gaussians clearly shows the presence of local orthorhombic regions with symmetry axes perpendicular to each other in the tetragonal phase. This local breaking of C_4 symmetry in the NMR spectrum is observed in $Ba(Fe_{1-x}Co_x)_2As_2$ [34–36], $BaFe_2(As_{1-x}P_x)_2$ [38], and $NaFe_{1-x}Co_xAs$ [37]. The analysis based on the two Gaussians may be consistent with a model

TABLE I. Weiss temperature T_η and constants C_η and η_0, obtained by fitting the data of the asymmetry parameter of the electric field gradient η to the Curie-Weiss law $\eta = C_\eta/(T - T_\eta) + \eta_0$ in the tetragonal phase of NaFeAs, LiFeAs, and $Ba(Fe_{1-x}Co_x)_2As_2$. The data of $Ba(Fe_{1-x}Co_x)_2As_2$ [36] are utilized for the present analysis.

Material	C_η (K)	T_η (K)	η_0
NaFeAs	0.68 ± 0.17	32 ± 8	0.0048 ± 0.0009
LiFeAs	0.60 ± 0.08	−142 ± 19	0.0002 ± 0.0002
$BaFe_2As_2$	0.98 ± 0.18	97 ± 8	0.0096 ± 0.0020
$Ba(Fe_{0.98}Co_{0.02})_2As_2$	2.4 ± 0.8	69 ± 14	0.016 ± 0.004
$Ba(Fe_{0.95}Co_{0.05})_2As_2$	7.6 ± 1.0	−3.6 ± 4.0	0.013 ± 0.006
$Ba(Fe_{0.92}Co_{0.08})_2As_2$	12 ± 4	−72 ± 33	0.017 ± 0.009

of fluctuating local orbital order with C_2 symmetry induced by an impurity, which was proposed by Inoue *et al.* [61]. They numerically obtained a fluctuating local orbital pattern, which forms two types of local orbital-order regions with the orthogonal Fe-Fe directions, in about $7a \times 15a$ lattice space. However, η is governed not by the orbital fluctuation but by the static orbital order. Therefore, η has to be zero in the tetragonal phase, which conflicts with the present observation of nonzero η in a no external stress condition. This conflict may be removed if a static nematic polarization proportional to the nematic susceptibility could be induced by internal stress due to a lattice imperfection, sample edge, etc., even in the absence of an external stress. This may be ascribed to the large nematic fluctuation in the tetragonal phase. The presence of nematic polarization is supported by a ^{77}Se NMR study, where spectrum broadening on short-range ordered nematicity in the tetragonal phase of FeSe [30,33] is discussed. The orbital ordering of Fe $3d_{xz}$ and d_{yz} electrons in the tetragonal phase of $BaFe_2(As_{1-x}P_x)_2$ from an ^{75}As NMR measurement [38] is discussed. The local nematic susceptibility is measured from the ^{75}As quadrupole splitting under a strain field in $BaFe_2As_2$ [39]. The presence of electronic nematicity is directly observed even at high temperatures in the tetragonal phase of NaFeAs by scanning tunneling microscopy [62].

If η could monitor the nematic susceptibility in the tetragonal phase, η has to obey the the CW law as observed in the electron Raman response and the shear modulus. Figure 6(a) shows the T dependence of η obtained by the present NMR experiments on NaFeAs and LiFeAs with the result of $BaFe_2As_2$ [36]. The η data can be well fitted by the CW law $\eta = C_\eta/(T - T_\eta) + \eta_0$ with constants C_η and η_0 and Weiss temperature T_η. The obtained C_η, T_η, and η_0 values are listed in Table I. This CW behavior is more clearly seen in Fig. 6(b), where $1/(\eta - \eta_0)$ vs T plots for NaFeAs, LiFeAs, and $BaFe_2As_2$ are displayed. It is also seen from the data of the tetragonal phase in the Co-doped $BaFe_2As_2$ system, $Ba(Fe_{1-x}Co_x)_2As_2$ [36], as presented in Figs. 6(c) and 6(d), which show the T dependences of η and $1/(\eta - \eta_0)$, respectively, for $x = 0$, 0.02, 0.05, and 0.08. The T_η, C_η, and η_0 values are also listed in Table I for $Ba(Fe_{1-x}Co_x)_2As_2$. In general, η has an on-site contribution η_{on} and a contribution coming from the surrounding ions $\eta_{lattice}$ as $\eta = \eta_{on} + \eta_{lattice}$. The hybridization between Fe $3d$ and As $4p$ orbitals provides η_{on}, which may be governed by the CW term of the nematic susceptibility, whereas $\eta_{lattice}$ due to local lowering from the

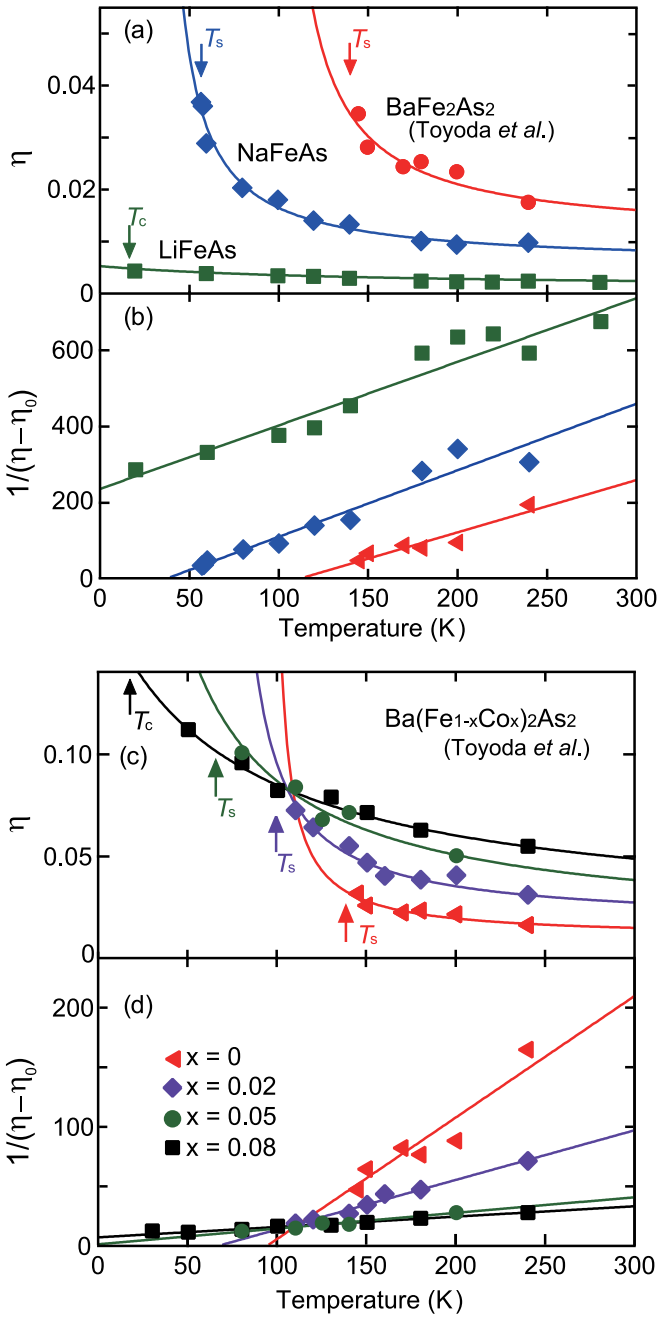

FIG. 6. (a) Asymmetry parameter of the electric field gradient η and (b) $1/(\eta - \eta_0)$ at the As site vs temperature in NaFeAs, LiFeAs, and $BaFe_2As_2$. (c) η and (d) $1/(\eta - \eta_0)$ vs temperature in $Ba(Fe_{1-x}Co_x)_2As_2$. The curves and straight lines are the results of fitting the data to the Curie-Weiss law $\eta = C_\eta/(T - T_\eta) + \eta_0$ with constants C_η and η_0, and the Weiss temperature T_η. The data of $Ba(Fe_{1-x}Co_x)_2As_2$ for the present analysis are from Ref. [36].

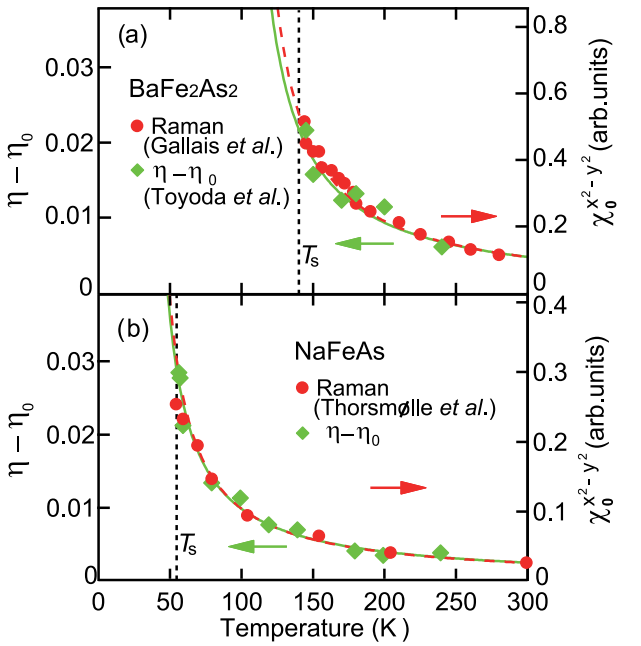

FIG. 7. Comparison between the asymmetry parameter of the electric field gradient $\eta - \eta_0$ and the Raman nematic susceptibility $\chi_0^{x^2-y^2}$ in (a) $BaFe_2As_2$ and (b) NaFeAs. The η data of $BaFe_2As_2$ are from Ref. [36], whereas the Raman data of $BaFe_2As_2$ and NaFeAs are quoted from Refs. [12] and [63], respectively. The solid and dashed curves are the results of fitting the experimental data to the Curie-Weiss law.

tetragonal symmetry may mainly contribute to η_0. On the other hand, below T_s, η shows T dependence obeying the order parameter of the nematic order in the paramagnetic orthorhombic phase of NaFeAs, as seen in Figs. 2(b) and 3(c). However, this T dependence of η above T_s is different from the previous report where η is zero above $T^* = 90$ K ($>T_s$) and obeys the relation $\eta \propto \sqrt{1 - T/T^*}$ below T^* [37]. If the lattice imperfection, etc., is large, the nematic order might appear due to an interaction between the neighboring nematic regions. The fact that the FWHM (∼0.48 MHz) of the satellite line in Ref. [37] is larger than 0.17 MHz at 100 K in the present sample seems to show a large amount of lattice imperfection, etc., in the former sample.

B. Comparison of η with Raman nematic susceptibility

The electronic Raman response can directly probe the weighted charge correlation function, which provides nematic susceptibility showing CW behavior [12]. Therefore, a comparison between η and Raman nematic susceptibility $\chi_0^{x^2-y^2}$ is useful to confirm whether or not the CW behavior of η is ascribed to nematic susceptibility. Figure 7 shows the $\eta - \eta_0$ vs $\chi_0^{x^2-y^2}$ plots for $BaFe_2As_2$ and NaFeAs where the available Raman nematic susceptibility data are from Refs. [12] and [63], respectively, and it is also noted that χ_0^{XY} in Ref. [63] corresponds to $\chi_0^{x^2-y^2}$ in this paper. The η data almost scale to the Raman nematic susceptibility data with a Weiss temperature T_0 of ∼100 K [12] and ∼33 K [63] for $BaFe_2As_2$ and NaFeAs, respectively. Also, T_η shows the x dependence to be in good agreement with that of T_0 [14] on the phase diagram of $Ba(Fe_{1-x}Co_x)_2As_2$ [64], as seen in Fig. 8.

As seen in Table I, NaFeAs and $BaFe_2As_2$ have positive T_η values in the CW behavior of η, whereas T_η of LiFeAs is negative. This characteristic behavior of η is related to the presence of a structural transition; namely, NaFeAs and $BaFe_2As_2$ undergo a structural transition at 54 and 140 K, respectively, whereas there is no structural transition in

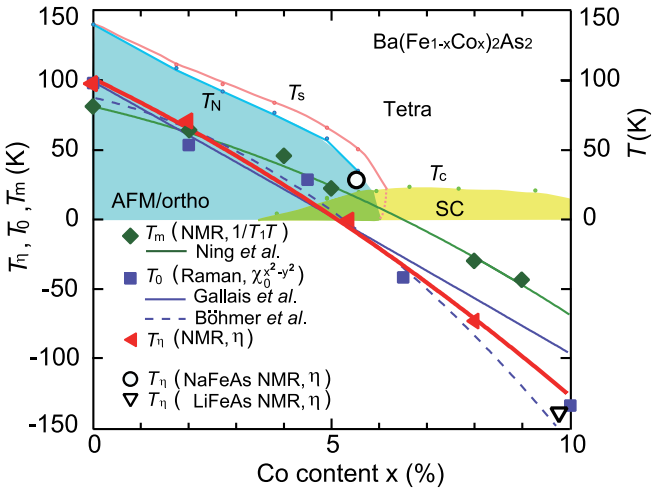

FIG. 8. Weiss temperature of the electric field gradient T_η vs x plot on the T-x phase diagram of $Ba(Fe_{1-x}Co_x)_2As_2$. Also, the Weiss temperature of the Raman nematic susceptibility T_0 [12] and that in $1/T_1T$, T_m [67], vs x plots in Ref. [12] are displayed for comparison. The solid curves are guides to the eye from Refs. [12,14]. In the phase diagram [64], T_s is the structural transition temperature from the tetragonal to orthogonal phases, T_N is the Néel temperature, and T_c is the superconducting (SC) transition temperature. The T_η data of NaFeAs and LiFeAs are effectively plotted on the phase diagram (see text).

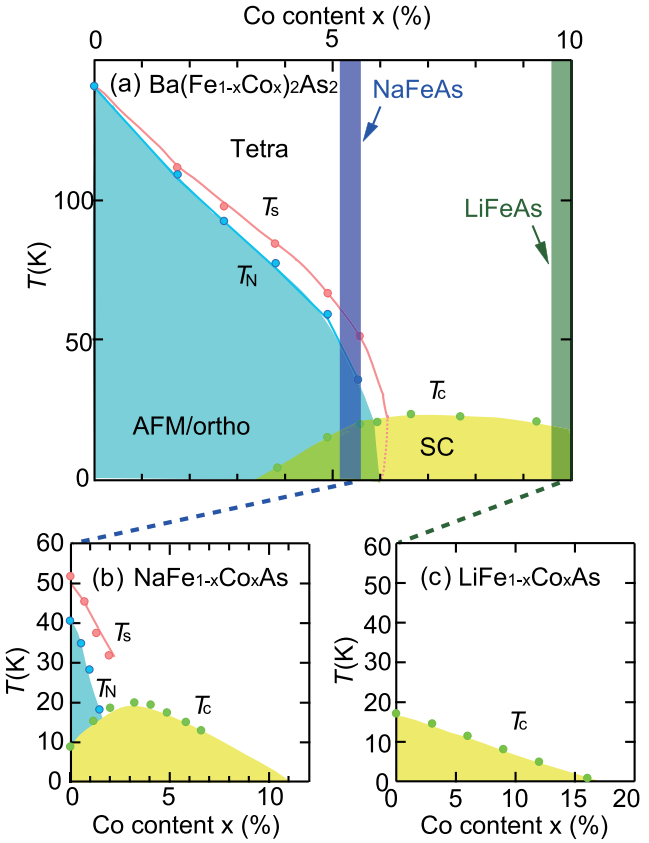

FIG. 9. Comparison of (a) the T-x phase diagram of $Ba(Fe_{1-x}Co_x)_2As_2$ [64] with (b) that of $NaFe_{1-x}Co_xAs$ [65] and (c) that of $LiFe_{1-x}Co_xAs$ [57]. In the phase diagrams, T_s is the structural transition temperature from the tetragonal to orthogonal phases, T_N is the Néel temperature, and T_c is the superconducting (SC) transition temperature. From comparing T_s and T_N (T_c) in NaFeAs (LiFeAs) with the transition temperatures in $Ba(Fe_{1-x}Co_x)_2As_2$, NaFeAs (LiFeAs) effectively corresponds to $x = 0.053$–0.058 (0.095–0.010) in $Ba(Fe_{1-x}Co_x)_2As_2$.

LiFeAs. This characteristic also appears in $Ba(Fe_{1-x}Co_x)_2As_2$, as seen in Fig. 8. The $x = 0.08$ sample with no structural transition has a negative T_η value. Furthermore, NaFeAs and LiFeAs can be effectively plotted on the phase diagram of $Ba(Fe_{1-x}Co_x)_2As_2$, as mentioned in the following. $NaFe_{1-x}Co_xAs$ has a SC phase with a maximum SC temperature $T_c = 19.5$ K [65], whereas the SC phase disappears above $x \sim 0.17$ in $LiFe_{1-x}Co_xAs$ [57], as presented in Fig. 9. There is a similarity between the phase diagram of $NaFe_{1-x}Co_xAs$ ($LiFe_{1-x}Co_xAs$) and that above $x \sim 0.053$ (0.095) in $Ba(Fe_{1-x}Co_x)_2As_2$. The similarity between the band structures of LiFeAs and $Ba(Fe_{0.92}Co_{0.08})_2As_2$ is also pointed out from the ARPES study [66]. Thus, comparing the T_s and T_N values in NaFeAs with those in $Ba(Fe_{1-x}Co_x)_2As_2$, NaFeAs effectively corresponds to $x = 0.053$–0.058 on the phase diagram of $Ba(Fe_{1-x}Co_x)_2As_2$. On the other hand, a comparison between the T_c values in LiFeAs and $Ba(Fe_{1-x}Co_x)_2As_2$ leads to that LiFeAs is effectively located at $x = 0.095$–0.100 on the phase diagram of the Co-doped Ba system. In Fig. 8, note that T_η is systematically dependent on the carrier concentration in the three systems. Also, the T_η values are lower than the T_s values, similar to the other Weiss temperatures of Raman susceptibility and C_{66} in $Ba(Fe_{1-x}Co_x)_2As_2$ [12]. This is explained by introducing a bilinear coupling between the nematic order parameter and the elastic strain in the Landau theory of the second-order transition [14]. Then, the difference between the Weiss temperature and T_s provides an energy scale characteristic of bilinear coupling. The fact that η becomes zero at $x \sim 0.05$ indicates the presence of a quantum critical point (QCP) in $Ba(Fe_{1-x}Co_x)_2As_2$ [14].

Thus we can conclude that η is able to monitor nematic susceptibility in Fe-based superconductors as well as Raman nematic susceptibility. This is desired to be clarified from a theoretical point of view.

C. Comparison of η with $1/T_1T$

The nematic susceptibility has been discussed from two aspects of the spin-nematic and the orbital-nematic origins. The spin-nematic origin comes from the instability of the two AFM fluctuations with $\mathbf{Q}_X$ and $\mathbf{Q}_Y$. On the other hand, Onari *et al.* showed that the Aslamazov-Larkin vertex correction induces nematic-type orbital fluctuations leading to the enhancement of Raman nematic susceptibility $\chi_0^{x^2-y^2}$ and the shear modulus C_{66} [23–25]. Thus it is useful to discuss the relation between η due to nematic fluctuations and $1/T_1T$ which probes the spin fluctuations. In $BaFe_2As_2$, $1/T_1T$ of ^{75}As shows the T dependence for $H_0 \perp c$, which was reported in Ref. [67], in Fig. 10(a). In Fe-based superconductors, the CW term $(1/T_1T)_{CW}$ in $1/T_1T = (1/T_1T)_{CW} + (1/T_1T)_{non\text{-}CW}$ is generally governed by AFM fluctuations. The non-CW term is phenomenologically introduced by several functions. In Refs. [63,67], $(1/T_1T)_{CW} = C_m/(T - T_m)$ with a constant

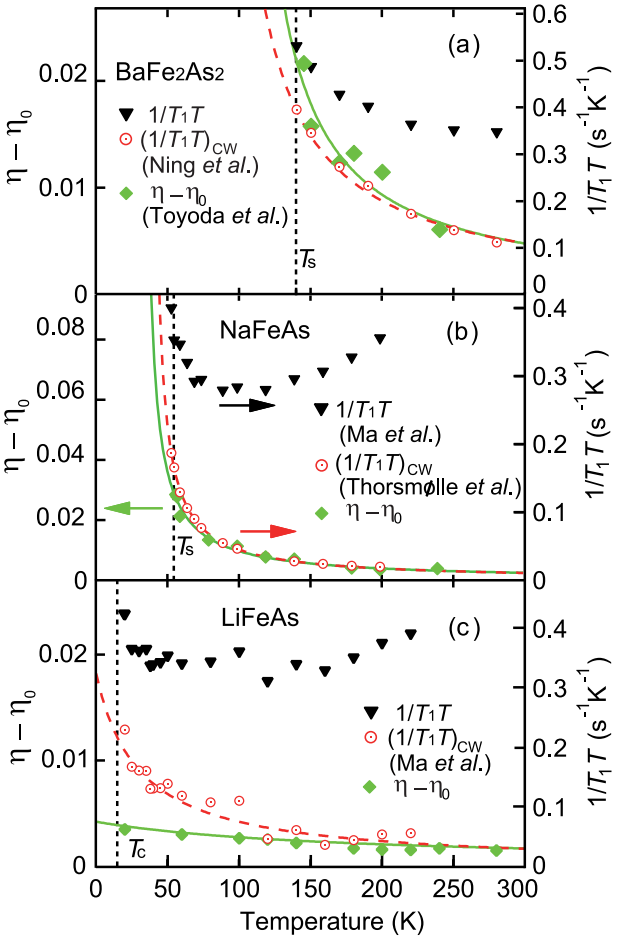

FIG. 10. Comparison between the T dependences of $\eta - \eta_0$ and $1/T_1T$ in (a) $BaFe_2As_2$, (b) NaFeAs, and (c) LiFeAs. The $1/T_1T$ data in $BaFe_2As_2$, NaFeAs, and LiFeAs are from Refs. [67], [49], and [53], respectively, whereas the η data in $BaFe_2As_2$ in Ref. [36] are utilized. The green solid curves are results of fitting the η data to the Curie-Weiss law $\eta = C_\eta/(T - T_\eta) + \eta_0$, whereas the red dashed curves are the CW terms obtained after fitting the $1/T_1T$ data to $1/T_1T = C_m/(T - T_m) + \alpha_0 + \beta_0 \exp(-\Delta/k_BT)$ for $BaFe_2As_2$ and NaFeAs, and $1/T_1T = A_0 + B_0T + C_m/(T - T_m)$ for LiFeAs (see text).

C_m and a Weiss temperature T_m was proposed to come from the interband contribution, whereas the intraband contribution was introduced as the non-CW term $(1/T_1T)_{\text{non-CW}} = \alpha_0 + \beta_0 \exp(-\Delta/k_BT)$, where α_0 and β_0 are constants, Δ is the gap due to intraband excitations, and k_B is the Boltzmann constant. In this model, the CW term provides $T_m = 78$ K for $BaFe_2As_2$ [67], whereas η shows $T_\eta = 97$ K, as presented by the curves in Fig. 10(a). In the Co-doped system $Ba(Fe_{1-x}Co_x)_2As_2$, $1/T_1T$ also shows CW behavior [67] with the x dependence of T_m, in agreement with that of η as seen in Fig. 8. From an analysis of the scaling between the nematic and the spin fluctuations, the main contribution to nematic susceptibility was concluded to be the spin fluctuations in $Ba(Fe_{1-x}Co_x)_2As_2$ [14]. The $1/T_1T$ data of ^{75}As in NaFeAs [49,51] and LiFeAs [53,57] are reported to show T dependence for $H_0 \perp c$, as presented in Figs. 10(b) and 10(c), respectively. In NaFeAs, $(1/T_1T)_{\text{CW}}$ denoted by the red dashed curve in Fig. 10(b) provides $T_m = 39$ K, which is obtained by fitting the $1/T_1T$ data to the above relation [51]. This CW behavior of $1/T_1T$ almost scales to the present η data with $T_\eta = 32$ K [63]. In LiFeAs, the $1/T_1T$ data are fitted by the relation $1/T_1T = A_0 + B_0T + C_m/(T - T_m)$, where the non-CW term is assumed as $(1/T_1T)_{\text{non-CW}} = A_0 + B_0T$ with constants A_0 and B_0 [49]. The obtained CW term with $T_m = -30$ K shown as the red dashed curve in Fig. 10(c) more largely deviates from the CW term of η with $T_\eta = -142$ K. Thus the present NMR results on $BaFe_2As_2$, NaFeAs, and LiFeAs seem to show the magnetic contribution to nematic susceptibility is material dependent. Furthermore, in FeSe which undergoes a structural transition and not a magnetic transition, $1/T_1T$ of ^{77}Se nuclei shows the absence of any measurable spin-fluctuation contribution above T_s [31]. This may mean that the spin fluctuations cannot be the origin of the structural transition. However, Yamakawa *et al.* proposed that the spin-fluctuation-mediated orbital order described by the Aslamazov-Larkin vertex correction takes place below T_s in spite of very weak spin fluctuations [68]. Thus the difference between the CW behaviors of η and $1/T_1T$ in $BaFe_2As_2$, NaFeAs, and LiFeAs may be explained by introducing the vertex correction.

D. Spin dynamics in NaFeAs

Finally, we turn our attention to the nematic order from η and the spin dynamics in the orthorhombic phase of NaFeAs. From the static point of view, we discuss the T dependence of η which is traced by the green dashed curve in Fig. 3(c). This curve is the result of fitting the data to the relation in the mean field approximation $\eta \propto \sqrt{1 - T/T_s}$ with $T_s = 57.0$ K. Thus η can well monitor an order parameter of the nematic order accompanied by the structural transition. Next, we have to take account of the local crystal structure to discuss the spin dynamics. The As site, which is located above or below the center of a rectangle which is formed by four neighboring Fe sites, is governed by the transferred hyperfine field coming from the neighboring Fe moments. The local structure provides useful information on the spin dynamics via the anisotropy of $1/T_1$, because $1/T_1T$ is governed by the spin fluctuations perpendicular to the applied magnetic field. This leads to equations of $1/T_1T$ expressed as [28,69]

$$(1/T_1T)_a^{\mathbf{Q}_X} \propto |A_{ac}|^2 \chi_a''(\mathbf{Q}_X,\omega_n),$$
$$(1/T_1T)_b^{\mathbf{Q}_X} \propto |A_{ac}|^2 \chi_a''(\mathbf{Q}_X,\omega_n) + |A_{ac}|^2 \chi_c''(\mathbf{Q}_X,\omega_n), \quad (3)$$

for the $\mathbf{Q} = \mathbf{Q}_X$ spin fluctuation and

$$(1/T_1T)_a^{\mathbf{Q}_Y} \propto |A_{bc}|^2 \chi_b''(\mathbf{Q}_Y,\omega_n) + |A_{bc}|^2 \chi_c''(\mathbf{Q}_Y,\omega_n),$$
$$(1/T_1T)_b^{\mathbf{Q}_Y} \propto |A_{bc}|^2 \chi_b''(\mathbf{Q}_Y,\omega_n), \quad (4)$$

for the $\mathbf{Q} = \mathbf{Q}_Y$ spin fluctuation, where $A_{\alpha\beta}$ $(\alpha,\beta = a,b,c)$ is the transferred hyperfine coupling constant, $\chi_\alpha''(\mathbf{Q}_j,\omega_n)$ is the imaginary part of dynamical susceptibility for $j = X$ and Y, and ω_n is the nuclear Larmor frequency. Above T_N, the spin fluctuations with $\mathbf{Q}_X$ and $\mathbf{Q}_Y$ contribute to $(1/T_1T)_\alpha$ as $(1/T_1T)_\alpha = N_{\mathbf{Q}_X}(1/T_1T)_\alpha^{\mathbf{Q}_X} + N_{\mathbf{Q}_Y}(1/T_1T)_\alpha^{\mathbf{Q}_Y}$, where $N_X + N_Y = 1$ [37]. By assuming $\chi_\alpha''(\mathbf{Q}_j,\omega_n) = \chi_\alpha''$ for $j = X$ and Y, and neglecting the anisotropy of the transferred hyperfine

coupling constants ($|A_{ac}| = |A_{bc}|$), the ratio $(1/T_1T)_b/(1/T_1T)_b$ is expressed as

$$\frac{(1/T_1T)_b}{(1/T_1T)_a} = \frac{\chi_c'' + \chi_a'' + f\chi_b''}{\chi_a'' + f(\chi_b'' + \chi_c'')}, \quad (5)$$

where $f = N_Y/N_X$ [37]. If the Q_X and Q_Y contributions are even ($N_X = N_Y$), $(1/T_1T)_b/(1/T_1T)_a = 1$. If the Q_X contribution is dominant ($N_X = 1$ and $N_Y = 0$), $(1/T_1T)_b/(1/T_1T)_a = 2$. As seen in Fig. 3(c), $(1/T_1T)_b/(1/T_1T)_a$ is slightly larger than unity above T_s, consistent with the nonzero η value. It increases down to ~48 K with decreasing T below T_s and obeys the T dependence of η. After $(1/T_1T)_b/(1/T_1T)_a$ reaches near two at ~48 K, it decreases toward one with decreasing T. This shows that the anisotropy of the low-energy spin dynamics in the c plane gradually vanishes with decreasing T below ~48 K. If the $\mathbf{Q}_X$ contribution becomes dominant (f becomes ~0) below ~48 K, the ratio almost obeys $1 + \chi_c''/\chi_a''$, as seen from Eq. (3). Thus χ_a'' has to become much larger than χ_c'' with a critical slowing down which appears toward T_N. This is reasonably expected by the AFM fluctuation leading to the stripe-type AFM order in the c plane below T_N. This characteristic spin excitation below ~48 K is consistent with the result of the inelastic neutron scattering study [70]. On the other hand, the T dependence of $(1/T_1T)_b/(1/T_1T)_a$ above T_s in NaFeAs is different from the reported result where it is zero above T^* ($>T_s$) and increases with decreasing T below T^* [37]. This difference may depend on whether or not there is nematic order in the tetragonal phase as discussed above.

V. CONCLUSION

We have performed ^{75}As NMR measurements on single crystals to study the nematic state in the iron arsenides NaFeAs and LiFeAs. The asymmetry of the electric field gradient η within the FeAs plane was found to exist even in the tetragonal phase of NaFeAs and LiFeAs as well as in $Ba(Fe_{1-x}Co_x)_2As_2$, clearly showing tetragonal C_4 symmetry breaking. Furthermore, η was observed to obey the Curie-Weiss law in the tetragonal phase. From comparing the η data with Raman nematic susceptibility, we concluded that η monitors the nematic susceptibility. Also, a comparison between the η and $1/T_1T$ data enabled us to conclude that the contribution of the spin fluctuation to nematic susceptibility is material dependent. We could clearly monitor the nematic order in the orthorhombic phase of NaFeAs from static and dynamical points of view. Thus NMR is able to be a useful probe to study the nematic fluctuation and the nematic order in Fe-based superconductors as well as the electron Raman spectroscopy and the shear modulus C_{66} measurement.

ACKNOWLEDGMENTS

We would like to thank H. Kontani and Y. Yamakawa for useful discussions, and S. Inoue for technical support. This study was supported by KAKENHI (Grants No. 15K05167 and No. 16H04012) from the Japan Society for the Promotion of Science. M.T. was supported by the Program for Leading Graduate Schools entitled "Integrative Graduate Education and Research Program in Green Natural Sciences."

[1] P. Dai, J. Hu, and E. Dagotto, Nat. Phys. **8**, 709 (2012).
[2] R. M. Fernandes, A. V. Chubukov, and J. Schmalian, Nat. Phys. **10**, 97 (2014).
[3] A. Chubukov and P. J. Hirschfield, Phys. Today **68** (6), 46 (2015).
[4] H.-H. Kuo, J.-H. Chu, J. C. Palmstrom, S. A. Kivelson, and I. R. Fisher, Science **352**, 958 (2016).
[5] J.-H. Chu, J. G. Analytis, K. De Greve, P. L McMahon, Z. Islam, Y. Yamamoto, and I. R. Fisher, Science **329**, 824 (2010).
[6] M. Yi, D. H. Lu, J.-H. Chu, J. G. Analytis, A. P. Sorinia, A. F. Kemper, B. Moritz, S.-K. Mod, R. G. Moore, M. Hashimoto, W.-S. Lee, Z. Hussain, T. P. Devereaux, I. R. Fisher, and Z.-X. Shen, Proc. Natl. Acad. Sci. USA **108**, 6878 (2011).
[7] R. M. Fernandes, L. H. Van Bebber, S. Bhattacharya, P. Chandra, V. Keppens, D. Mandrus, M. A. McGuire, B. C. Sales, A. S. Sefat, and J. Schmalian, Phys. Rev. Lett. **105**, 157003 (2010).
[8] T. Goto, R. Kurihara, K. Araki, K. Mitsumoto, M. Akatsu, Y. Nemoto, S. Tatematsu, and M. Sato, J. Phys. Soc. Jpn. **80**, 073702 (2011).
[9] M. Yoshizawa, D. Kimura, T. Chiba, S. Simayi, Y. Nakanishi, K. Kihou, K. C.-H. Lee, A. Iyo, H. Eisaki, M. Nakajima, and S. Uchida, J. Phys. Soc. Jpn. **81**, 024604 (2012).
[10] A. E. Böhmer, P. Burger, F. Hardy, T. Wolf, P. Schweiss, R. Fromknecht, M. Reinecker, W. Schranz, and C. Meingast, Phys. Rev. Lett. **112**, 047001 (2014).
[11] J.-H. Chu, H.-H. Kuo, J. G. Analytis, and I. R. Fisher, Science **337**, 710 (2012).
[12] Y. Gallais, R. M. Fernandes, I. Paul, L. Chauviere, Y.-X. Yang, M.-A. Méasson, M. Cazayous, A. Sacuto, D. Colson, and A. Forget, Phys. Rev. Lett. **111**, 267001 (2013).
[13] C. Mirri, A. Dusza, S. Bastelberger, J.-H. Chu, H.-H. Kuo, I. R. Fisher, and L. Degiorgi, Phys. Rev. B **89**, 060501 (2014).
[14] A. E. Böhmer and C. Meingast, C. R. Phys. **17**, 90 (2016).
[15] F. Wang, S. A. Kivelson, and D.-H. Lee, Nat. Phys. **11**, 959 (2015).
[16] A. V. Chubukov, R. M. Fernandes, and J. Schmalian, Phys. Rev. B **91**, 201105 (2015).
[17] R. Yu and Q. Si, Phys. Rev. Lett. **115**, 116401 (2015).
[18] J. K. Glasbrenner, I. I. Mazin, H. O. Jeschke, P. J. Hirschfeld, and R. Valenti, Nat. Phys. **11**, 953 (2015).
[19] L. Fanfarillo, A. Cortijo, and B. Valenzuela, Phys. Rev. B **91**, 214515 (2015).
[20] F. Krüger, S. Kumar, J. Zaanen, and J. van den Brink, Phys. Rev. B **79**, 054504 (2009).
[21] W. Lv, J. Wu, and P. Phillips, Phys. Rev. B **80**, 224506 (2009).
[22] C.-C. Lee, W.-G. Yin, and W. Ku, Phys. Rev. Lett. **103**, 267001 (2009).
[23] S. Onari and H. Kontani, Phys. Rev. Lett. **109**, 137001 (2012).
[24] S. Onari, Y. Yamakawa, and H. Kontani, Phys. Rev. Lett. **112**, 187001 (2014).
[25] S. Onari and H. Kontani, in *Iron-Based Superconductivity* edited by P. D. Johnson, G. Xu, and W.-G. Yin (Springer, Berlin, 2015).
[26] K. Jiang, J. P. Hu, H. Ding, and Z. Wang, Phys. Rev. B **93**, 115138 (2016).

[27] K. Ishida, Y. Nakai, and H. Hosono, J. Phys. Soc. Jpn. **78**, 062001 (2009), and references therein.

[28] L. Ma and W.-Q. Yu, Chin. Phys. B **22**, 087414 (2013), and references therein.

[29] S.-H. Baek, D. V. Efremov, J. M. Ok, J. S. Kim, J. van den Brink, and B. Büchner, Nat. Mater. **14**, 210 (2015).

[30] S.-H. Baek, D. V. Efremov, J. M. Ok, J. S. Kim, J. van den Brink, and B. Büchner, Phys. Rev. B **93**, 180502(R) (2016).

[31] A. E. Böhmer, T. Arai, F. Hardy, T. Hattori, T. Iye, T. Wolf, H. V. Löhneysen, K. Ishida, and C. Meingast, Phys. Rev. Lett. **114**, 027001 (2015).

[32] P. S. Wang, P. Zhou, S. S. Sun, Y. Cui, T. R. Li, H. Lei, Z. Wang, and W. Yu, Phys. Rev. B **96**, 094528 (2017).

[33] P. Wiecki, M. Nandi, A. E. Böhmer, S. L. Bud'ko, P. C. Canfield, and Y. Furukawa, Phys. Rev. B **96**, 180502(R) (2017).

[34] Y. Kobayashi, A. Ichikawa, M. Toyoda, M. Itoh, and M. Sato, J. Korean Phys. Soc. **63**, 481 (2013).

[35] M. Toyoda, Y. Kobayashi, M. Itoh, and M. Sato, J. Phys.: Conf. Ser. **568**, 022029 (2014).

[36] M. Toyoda, A. Ichikawa, Y. Kobayashi, M. Sato, and M. Itoh (unpublished).

[37] R. Zhou, L. Y. Xing, X. C. Wang, C. Q. Jin, and G.-Q. Zheng, Phys. Rev. B **93**, 060502(R) (2016).

[38] T. Iye, M.-H. Julien, H. Mayaffre, M. Horvatić, C. Berthier, K. Ishida, H. Ikeda, S. Kasahara, T. Shibauchi, and Y. Matsuda, J. Phys. Soc. Jpn. **84**, 043705 (2015).

[39] T. Kissikov, R. Sarkar, M. Lawson, B. T. Bush, E. I. Timmons, M. A. Tanatar, R. Prozorov, S. L. Bud'ko, P. C. Canfield, R. M. Fernandes, W. F. Goh, W. E. Pickett, and N. J. Curro, Phys. Rev. B **96**, 241108(R) (2017).

[40] A. P. Dioguardi, M. M. Lawson, B. T. Bush, J. Crocker, K. R. Shirer, D. M. Nisson, T. Kissikov, S. Ran, S. L. Bud'ko, P. C. Canfield, S. Yuan, P. L. Kuhns, A. P. Reyes, H.-J. Grafe, and N. J. Curro, Phys. Rev. B **92**, 165116 (2015).

[41] T. Kissikov, A. P. Dioguardi, E. I. Timmons, M. A. Tanatar, R. Prozorov, S. L. Bud'ko, P. C. Canfield, R. M. Fernandes, and N. J. Curro, Phys. Rev. B **94**, 165123 (2016)

[42] A. P. Dioguardi, T. Kissikov, C. H. Lin, K. R. Shirer, M. M. Lawson, H.-J. Grafe, J.-H. Chu, I. R. Fisher, R. M. Fernandes, and N. J. Curro, Phys. Rev. Lett. **116**, 107202 (2016).

[43] J. H. Tapp, Z. Tang, B. Lv, K. Sasmal, B. Lorenz, P. C. W. Chu, and A. M. Guloy, Phys. Rev. B **78**, 060505(R) (2008).

[44] D. R. Parker, M. J. Pitcher, P. J. Baker, I. Franke, T. Lancaster, S. J. Blundell, and S. J. Clarke, Chem. Commun. 2189 (2009).

[45] S. Li, C. de la Cruz, Q. Huang, G. F. Chen, T.-L. Xia, J. L. Luo, N. L. Wang, and P. C. Dai, Phys. Rev. B **80**, 020504(R) (2009).

[46] M. J. Pitcher, D. R. Parker, P. Adamson, S. J. C. Herkelrath, A. T. Boothroyd, R. M. Ibberson, M. Brunelli, and S. J. Clarke, Chem. Commun. 5918 (2008).

[47] K. Kitagawa, Y. Mezaki, K. Matsubayashi, Y. Uwatoko, and M. Takigawa, J. Phys. Soc. Jpn. **80**, 033705 (2011).

[48] M. Klanjšek, P. Jeglič, B. Lv, A. M. Guloy, C. W. Chu, and D. Arčon, Phys. Rev. B **84**, 054528 (2011).

[49] L. Ma, G. F. Chen, D.-X. Yao, J. Zhang, S. Zhang, T.-L. Xia, and W. Yu, Phys. Rev. B **83**, 132501 (2011).

[50] K. Kitagawa, Y. Mezaki, K. Matsubayashi, Y. Uwatoko, and M. Takigawa, JPS Conf. Proc. **3**, 015031 (2014).

[51] L. Ma, J. Dai, P. S. Wang, X. R. Lu, Y. Song, C. Zhang, G. T. Tan, P. Dai, D. Hu, S. L. Li, B. Normand, and W. Yu, Phys. Rev. B **90**, 144502 (2014).

[52] P. Jeglič, A. Potočnik, M. Klanjšek, M. Bobnar, M. Jagodič, K. Koch, H. Rosner, S. Margadonna, B. Lv, A. M. Guloy, and D. Arčon, Phys. Rev. B **81**, 140511(R) (2010).

[53] L. Ma, J. Zhang, G. F. Chen, and W. Yu, Phys. Rev. B **82**, 180501(R) (2010).

[54] Z. Li, Y. Ooe, X.- C Wang, Q.-Q. Liu, C.-Q. Jin, M. Ichioka, and G.-Q. Zheng, J. Phys. Soc. Jpn. **79**, 083702 (2010).

[55] S.-H. Baek, H.-J. Grafe, F. Hammerath, M. Fuchs, C. Rudisch, L. Harnagea, S. Aswartham, S. Wurmehl, J. van den Brink, and B. Büchner, Eur. Phys. J. B **85**, 159 (2012).

[56] S.-H. Baek, L. Harnagea, S. Wurmehl, B. Büchner, and H.-J. Grafe, J. Phys.: Condens. Matter **25**, 162204 (2013).

[57] Y. M. Dai, H. Miao, L. Y. Xing, X. C. Wang, P. S. Wang, H. Xiao, T. Qian, P. Richard, X. G. Qiu, W. Yu, C. Q. Jin, Z. Wang, P. D. Johnson, C. C. Homes, and H. Ding, Phys. Rev. X **5**, 031035 (2015).

[58] I. Morozov, A. Boltalin, O. Volkova, A. Vasiliev, O. Kataeva, U. Stockert, M. Abdel-Hafiez, D. Bombor, A. Bachmann, L. Harnagea, M. Fuchs, H.-J. Grafe, G. Behr, R. Klingeler, S. Borisenko, C. Hess, S. Wurmehl, and B. Büchner, Cryst. Growth Des. **10**, 4428 (2010).

[59] A. Abragam, *Principles of Nuclear Magnetism* (Oxford University Press, Oxford, UK, 1961).

[60] E. R. Andrew and D. P. Tunstall, Proc. Phys. Soc. **78**, 1 (1961).

[61] Y. Inoue, Y. Yamakawa, and H. Kontani, Phys. Rev. B **85**, 224506 (2012).

[62] E. P. Rosenthal, E. F. Andrade, C. J. Arguello, R. M. Fernandes, L. Y. Xing, X. C. Wang, C. Q. Jin, A. J. Millis, and A. N. Pasupathy, Nat. Phys. **10**, 225 (2014).

[63] V. K. Thorsmølle, M. Khodas, Z. P. Yin, C. Zhang, S. V. Carr, P. Dai, and G. Blumberg, Phys. Rev. B **93**, 054515 (2016).

[64] S. Nandi, M. G. Kim, A. Kreyssig, R. M. Fernandes, D. K. Pratt, A. Thaler, N. Ni, S. L. Bud'ko, P. C. Canfield, J. Schmalian, R. J. McQueeney, and A. I. Goldman, Phys. Rev. Lett. **104**, 057006 (2010).

[65] A. F. Wang, X. G. Luo, Y. J. Yan, J. J. Ying, Z. J. Xiang, G. J. Ye, P. Cheng, Z. Y. Li, W. J. Hu, and X. H. Chen, Phys. Rev. B **85**, 224521 (2012).

[66] V. Brouet, D. LeBoeuf, P.-H. Lin, J. Mansart, A. Taleb-Ibrahimi, P. Le Fèvre, F. Bertran, A. Forget, and D. Colson, Phys. Rev. B **93**, 085137 (2016).

[67] F. L. Ning, K. Ahilan, T. Imai, A. S. Sefat, M. A. McGuire, B. C. Sales, D. Mandrus, P. Cheng, B. Shen, and H.-H. Wen, Phys. Rev. Lett. **104**, 037001 (2010).

[68] Y. Yamakawa, S. Onari, and H. Kontani, Phys. Rev. X **6**, 021032 (2016).

[69] K. Kitagawa, N. Katayama, K. Ohgushi, and M. Takigawa, J. Phys. Soc. Jpn. **78**, 063706 (2009).

[70] J. Liu, J. Wang, W. Luo, J. Sheng, A. Wang, X. Chen, S. A. Danilkin, and W. Bao, J. Phys.: Condens. Matter **28**, 27LT01 (2016).